Revista Mexicana de Física 37 No. 2(1991) 201-229

The physical properties of donor states in germanium

Hugo R. Navarro C. and M.A. Palomino Ovando

Instituto de Física Luis Rivera Terrazas
Universidad Autónoma de Puebla
Apartado postal J-48, 72570 Puebla, Pue., México

(Recibido el 9 de mayo de 1990; aceptado el 22 de noviembre de 1990)

Abstract. A survey of physical properties related to the optical observation of transitions between electronic quantum states of donor impurities in the semiconductor material germanium is presented in this work. Emphasis is laid on the interplay that far infrared spectroscopy and the effective mass model have had in this subject in order to observe and predict with high precision the energy distribution of their quantum states, and how this knowledge of the quantum nature of these states can be used to calculate their response to applied or incident fields. Some of the phenomena discussed are illustrated by the presentation of previously unpublished experimental and theoretical results: these are the saturation of the absorption coefficient of donor transitions and the theoretical calculation of the Zeeman response of $2P_{\pm}$, $3P_{\pm}$ and $4P_{\pm}$ donor levels. The physical agents that affect the linewidth of donor transitions are discussed. Intrinsic linewidth measurements are reinterpreted as being determined by the envelope of the resultant coupled bound electron-phonon states due to the electron-acoustic phonon interaction at temperatures different from zero Kelvin.

PACS: 78.50.-w

1. Introduction

The semiconductor germanium, discovered just one century ago [1], together with its partner in column IV of the Periodic Table of the Chemical Elements, silicon, belong to the class of the best understood solids [2]. Ge can be grown in the form of large single crystals up to 100 Kg in weight with exceptional perfection and purity. Germanium single crystals have been grown with one electrically active impurity in 4×10^{13} host atoms [2,3], *i.e.*, in concentrations $\leq 10^9$ cm^{-3}, clasifiying it as the most pure solid substance prepared by man. The incentive to prepare ultra-pure Ge was driven by the need for larger, better, and more stable gigantic gamma ray detector diodes which require net-dopant concentrations of the order of 10^{10} cm^{-3} or less [4]. Hence, single crystal, ultra-pure Ge forms an ideal semiconductor matrix to study a host of physical phenomena intrinsic to the solid state and to check our theoretical understanding of them.

Among many other interesting physical phenomena existing in semiconductors, the study of donor impurities has benefited from the availability of ultra-pure Ge. A donor impurity is one which has one or several loosely bound electrons at $T = 0$ K. The best known examples of donor impurities in Ge are the elements of the V column of the Periodic Table, P, As and Sb [5]. These enter as pentavalent, substitutional impurities in place of Ge atoms. Four of its five valence electrons form covalent bonds with the tetrahedrally oriented valence electrons of the four nearest neighbour Ge atoms. The fifth electron remains unmatched and hence very loosely bound, with binding energies E_b of the order of 10 meV, *i.e.*, two orders of magnitude smaller than those associated with the covalent bonds. This electron is easily ionized, either thermally or by incident light. When freed, it contributes as a "donated" extra carrier to the electrical conductivity of the semiconductor. A similar physical but complementary situation exists for the chemical elements of the third column of the Periodic Table, B, Al, Ga and In in Ge, where the missing fourth electron serves as an empty receptacle of one electron of some neighbouring Ge atom leaving behind a "hole" which can propagate through many Ge atoms. These types of impurities are then ready to accept an extra electron forming what are called "Acceptor" impurities [5]. The holes created in this way behave for many purposes as effective positive carriers. They are also loosely bound, with binding energies of $E_b = 25$ meV. The great importance of impurity states in determining the room temperature electrical conductivities of all known semiconductor materials [6,7] was recognized very early in the development of Solid State theory.

Being donor (or acceptor) impurities known for a such long time, one may ask what is the reason for devoting time and efforts at the present time to their study. The answer is that, since the fifties, there have been many developments in solid state spectroscopy techniques which together with the improvements in the degree of refinement with which Si, Ge or many other semiconductors can be grown have revealed a wealth of interesting physical phenomena asociated with these donor or acceptor states. Hence, nowadays, there is a continuous effort to probe and explain the new physical features that donors have revealed [2,3]. Two spectroscopical techniques have played very significant roles in the unraveling of the physical features of donors: far-infrared (FI) Fourier Transform Spectroscopy (FTS) [2,8] and the development of far-infrared CO_2-laser-pumped alcohol lasers [9]. These two techniques allow the experimentalists to tune to the spectral region where the electronic transitions from the ground to excited states of donor (acceptor) impurities take place, corresponding to energies $\Delta E \simeq 10$ meV, or less, *i.e.*, $\lambda \simeq 100$ μm or larger wavelengths well inside the FI region. These two spectroscopical tools have very large resolution allowing access to the wealth of electronic transitions between donor (acceptor) states and all related physical parameters pertinent to these transitions: the photon absorption and photoionization cross sections, the recapture and relaxation process of electrons to the ground state (GS) by the ionized donor, the life and relaxation times involved, the response fo donor states to applied fields, etc.

The subject of this work is to discuss and illustrate with relevant experimental results the present knowledge of the donors in Ge and to introduce and review our

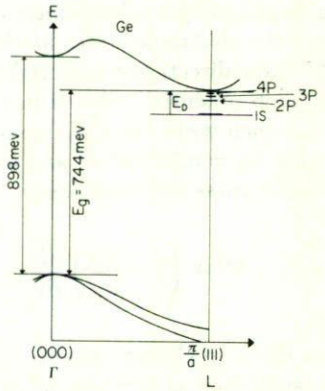

FIGURE 1. Donor states associated with the minimum of the conduction band in germanium.

contributions to the understanding of the nature of some of its physical parameters. We present new results that illustrate the donor phenomenology on two subjects: A study of the saturation process of the absorption coefficient corresponding to transitions from the GS to the electronic continuum for the Sb donor in Ge. This experiment provides insight into the extensive collection of phenomena known for donor states. The second is a theoretical study of the Zeeman response of donor transitions that provides a satisfactory explanation to the effects observed for the D(H, O) donor under applied magnetic fields $\leq$ 4.5 KOe.

2. The physical processes that determine the absorption of photons by electrons in donor states

2.1. Donor quantum states: the Effective Mass Theory

The simplest picture that one can imagine for the single electron of an elementary donor, *i.e.* those formed by P, As and Sb in Ge, is that of one electron orbiting somewhat far away from the positively charged central impurity ion in the Coulomb field that it produces. This simple hydrogen-like picture is the basis for a more sophisticated model: the Effective Mass Theory (EMT) which has been very successful in describing the series of observed excited states of donor impurities [3,7,10,11,12]. In what follows we describe briefly the essential elements of the EMT and comment briefly the most relevant articles which describe it.

2.1.a. The Effective Mass Theory (EMT) Donor Hamiltonian. The effective mass theory was developed by Kittel and Mitchell [10] and by Kohn and Luttinger [11] in the mid-1950's. It takes into consideration that a donor state is formed in k–space associated with the lowest minimum of the conduction band of the semiconductor being studied, Fig. 1. In these works, [7,10,11] it is shown that the

donor electronic states are described by a Schroedinger equation in which the kinetic term corresponds to that of the electronic states at the bottom of the conduction band, with the appropiate three-directional tensorial components of the effective electronic mass and a Coulomb potential reduced in strength by the macroscopic dielectric constant ϵ. We can then write the effective-mass Hamiltonian for donors in germanium in atomic units $R_y = m_t^* e^4/2\hbar^2\epsilon^2$ and $a = \epsilon\hbar^2/m_t^* e^2$, with m_t^* being the effective transverse electron mass discussed below, as

$$H_0 = -\nabla^2 + \left(1 - \frac{m_t}{m_l}\right)\frac{\partial^2}{\partial z^2} - \frac{2}{r}. \tag{1}$$

The appearance of two effective electron masses, m_t and m_l in this equation, reflects the physical observation that at the bottom of the conduction band there are two distinguishible crystallographic directions (parallel and perpendicular to the four equivalent [111] directions) along which the electrons in this conduction valley manifest two different masses, as observed in the famous experiments of the cyclotron resonance of electrons in n–type Ge [13,14,15]. They have the values $m_t = 0.08152 m_e$ and $m_l = 1.588 m_e$, Ref [14]. The constant-energy surfaces of electrons in these CB minima have the well known geometrical figure of a prolate-spheroid [5]. In Ge there are four equivalent such CB minima to which donor states associate.

The donor Rydberg energy is usually taken as the binding energy, which in terms of the hydrogen Rydberg is written as

$$E_b = 13.6 \text{ eV } m^*/\epsilon^2 m_e; \qquad \text{while} \qquad a = (\epsilon m_e/m^*)a_0 \tag{2}$$

is the effective donor Bohr radius. The typical relative dielectric constant ϵ of a semiconductor has a value ≥ 10 which leads to a reduction of E_b by more than two orders of magnitude. Furthermore, the effective electron mass is typically another order of magnitude smaller, at least for Ge, producing a net reduction of E_b of three orders of magnitude to give $E_b \simeq 10$ meV as mentioned before. In the same manner we can see that with $\epsilon = 16.0$ for Ge, the Bohr radius of a donor is $a \cong 80$ Å *i.e.*, around 160 times larger than for the hydrogen atom.

The theoretical calculations of the binding energies of the donor states predicted by equation (1) were carried out by Kohn and Luttinger [11], Faulkner [12] and recently by Broeckx, Clauws and Vennik [16]. We will give a short discussion of the essential elements of their calculations and compare with the observed binding energies of the best kwnown donors in Ge.

Inspection of the Hamiltonian (1), shows that it is invariant under the operations of inversion, rotation about the z axis and time reversal. Thus the donor eigenfunctions have a well defined even or odd parity, the z–component eingenvalues of the angular momentum operator L_z are good quantum numbers for them, and by the time-reversal invariance these magnetic quantum numbers m and $-m$ are degenerate. Thus, for a p state, the levels, which for the hydrogen Hamiltonian are degenerate, now split into a singlet p_0 with $m = 0$ and a doublet $p_\pm$ with $m = \pm 1$.

In addition, as already stated there are four equivalent positions in the Brillouin zone for the conduction band minimum. For each of these positions we must solve the Hamiltonian (1), bearing in mind that, while the structure of the differential equation remains the same, the z direction is different for each minimum. Arising from this consideration all donor states exhibit a four-fold degeneracy in Ge in the framework of the EMT.

The EMT Hamiltonian (1) does not distinguish between the chemical nature of the different donor impurities, *i.e.* if it did, it would be the end of the story because there would not be a spectroscopical way to differentiate between the set of known impurities which have donor properties. However, two physical facts affect this degeneracy allowing the chemical identification of donors: the crystal potential *i.e.* the resultant electrostatic potential due to the symmetrical distribution of the ions of the lattice applied to the donor energy levels, and second, because of the fact that the ground state function, $1S$-like, has a probability different from zero at the position of the nucleus of the impurity, it becomes particularly sensitive to the actual specific details of the chemical ionic potential. The net effect is very pronounced for the ground state, it shifts to deeper energies and it splits for the case of Ge into a singlet $1S(A_1)$, the actual GS, and a triplet $1S(T_2)$. Here A_1 and T_2 are labels corresponding to different irreducible representations of the tetrahedral symmetry point group T_d which contains all the symmetry operations which leave invariant the configuration of the subtitutional place ocuppied by the impurity atoms.

The decomposition of the $1S$ multiplet into its components is referred in the literature [17] as "valley-orbit" or "chemical" splitting, the shift is called the "chemical shift". The calculated effect of these two physical factors is negligible for the whole set of excited states, with the exception fo the four 2S states where a very small effect similar to that of the 1S multiplet is expected, yet so far not detected for any donor in Ge. This chemical shift, different for each type of donor is a very fortunate event for the spectroscopists: the sequence of transitions are identical in energy separation for *all donors* but they are shifted with respect to the origin of energies allowing a clear identification of the different types of donors, Fig. 2.

2.1.b. Solution of the EMT Donor Hamiltonian. The first attempt to solve the EMT donor Hamiltonian to obtain the binding energies of the GS and some of the first excited states was that of Kohn and Luttinger [11]. They used modified hydrogen wavefunctions (WF) by substituting the variable r by its "prolate ellipsoidal" version $r^2 = (x^2 + y^2)/a^2 + z^2/b^2$, where a and b represent modified "donor Bohr radii". Both a and b were used as variational parameters, different for each WF. They calculated the binding energies of the first two even- and odd-parity levels with $m = 0$ $(1S, 2S, 2P_0, 3P_0)$ and those of the first odd-parity state with $m = \pm 1(2P_{\pm 1})$ for the mass ratio parameter $\gamma = m_t/m_l$ and for $0 \leq \gamma \leq 1$. A different variational method was used by Faulkner [12] to calculate, as a function of the same range of γ values, the energies of the first nine levels in each of the series of S-like, P_0-like and $P_{\pm 1}$-like states. His approach consists of substituting in the associated-Laguerre functions of the radial hydrogen WF's the z variable by the expression $(\beta/\gamma)^{1/2} z$

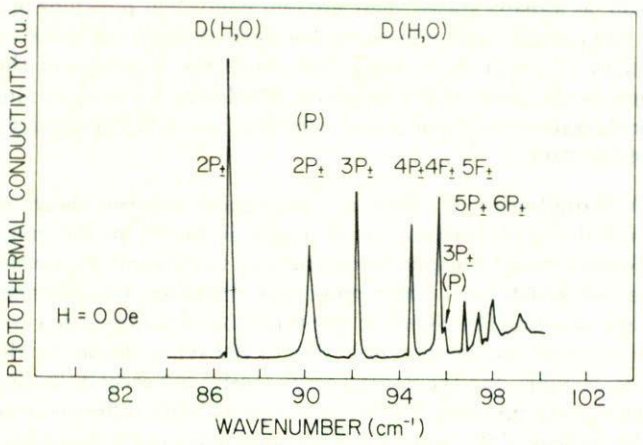

FIGURE 2. Spectral transition lines in the far infrared corresponding to two different donors in Ge: phosphorous and the D(H, O), hydrogen-oxygen donor center, showing how the same quantum transitions are spectroscopically well separated in energy.

and a prefactor of the WF $(\beta/\gamma)^{1/4}$ where β is a variational parameter for each set of same (l, m), but different n WF's.

Faulkner's calculations, Table I, stood for a long time as a successful and useful set of accurate calculations for the donor states in both Ge and Si. These have been used to assign and label the experimentally observed transition lines. A recent calculation by Broeckx *et al.* [16], referred here to as BCV, provides improved accuracy for the binding energies of the donor states. BCV used a quickly converging variational method devised by Lipari and Baldereschi [18] to solve for acceptor states in cubic-symmetric valence band semiconductors (such as Si and Ge) to solve the EMT donor Hamiltonian. Their results are also listed in Table I for comparison. It can be seen that they calculated the binding energies of the first 35 consecutive donor excited states. Their results have been seldom used but undoubtedly they will gain more acceptance in the future because they fit far more accurately the observed even-parity states. [19] For the odd-parity $5P_{\pm 1}$ state observed with binding energy of 0.47 ± 0.01 meV they predict it correctly in contrast to Faulkner, who calculates for the same level identified as $5F_{\pm}$, 0.41 meV, a difference in energy which is significant in the FIR spectroscopy of these donors in Ge, Fig. 2.

2.1.c. Experimental donor spectra. In Fig. 2 is shown the spectrum of one of the donors with *the sharpest transition lines observed for electronic state transitions in Solid State Physics*, the hydrogen-oxygen donor [20,21,22] D(H, O) in Ge. The typical linewidth measured for its observed transitions is 8 μeV. [22]

In Fig. 2 seven strong and well defined transitions of the D(H, O) donor are visible. In this donor above 6 K other identical series of transition lines are visible at smaller energies, of strongly temperature dependent strength, originating from thermally populating one of the split $1S$ states [21], allowing the spectroscopical

THEORY				EXPERIMENTAL									
Brockx, Clauws & Vennik		Faulkner		P [24,25]	Sb [24]	As [25]	Bi [25]	Li [2]	D(LI,O) [2]	D(H,O) [2,21]	O thermal donors a	b	c
$2P_0$	4.78	$2P_0$	4.741	4.73	4.75	4.74	4.76	4.75					
$2S$	3.60	$2S$	3.52		3.60								
$3P_0$	2.59	$3P_0$	2.559	2.56	2.56	2.57	2.56	2.56					
$2P_\pm$	1.73	$2P_\pm$	1.726	1.73	1.73	1.73	1.68	1.73	1.726	1.726	1.73	1.73	1.73
$4P_0$	1.70	$4P_0$	1.67		1.67								
$3S$	1.48	$3P_0$	1.34		1.42								
$3D_{\pm1}$	1.27				1.25								
$3P_{\pm1}$	1.04	$3P_\pm$	1.035	1.04	1.03	1.02	1.04	1.038	1.043	1.042			
$4D_{\pm1}$	0.87				0.85								
$4F_{\pm1}$	0.75	$4P_\pm$	0.73	0.75	0.74			0.753	0.756	0.758			
$5G_{\pm1}$	0.65				0.63								
$4P_\pm$	0.61	$4F_\pm$	0.61	0.62	0.59			0.606	0.612	0.613			
$6H_0$	0.58	$6F_0$	0.55										
$5F_{\pm1}$	0.57	$5P_\pm$	0.53		0.58								
$5D_\pm$	0.51				0.51								
$5P_{\pm1}$	0.47	$5F_\pm$	0.41	0.47	0.46			0.466	0.481	0.477			
$6H_{\pm1}$	0.40	$6P_\pm$	0.38	0.40	0.39			0.403	0.405	0.407			
$6F_{\pm1}$	0.38	$6F_\pm$	0.32										
$6P_{\pm1}$	0.32	$6H_\pm$	0.29	0.32	0.32				0.329	0.331			
$7H_{\pm1}$	0.31				0.30								
$7F_{\pm1}$	0.29												
$1S(A_1)$		$1S(A_1)$	9.81	12.88	10.45	14.18	12.75	10.012	10.462		17.28	17.6	18.1
$1S(T_2)$		$1S(T_2)$	9.81	10.06	10.32	9.44	9.90						
$1S(\Gamma_1+\Gamma_5)$										12.462			
$1S(\Gamma_1+\Gamma_5)$										10.89			
$1S(\Gamma_4+\Gamma_5)$										10.52			

TABLE I. Binding energies of the energy levels of donors in Ge (meV).

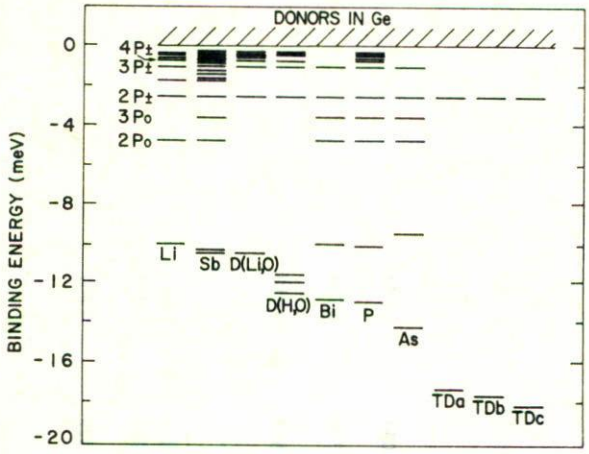

FIGURE 3. Schematics of the binding energies of different donor centers in Ge.

determination of its binding energy. Although the transitions measured are sharper, this spectrum is identical in the series of observed lines to those recorded in the literature for other donor impurities, *i.e.*, for P, [23] Sb, [23] As, [24] Bi, [24] Li, [25] Li-O, [26] and similar to those of the series of oxygen thermal donors (TD) in Ge, [27] Table I.

As a final comment, one can say that the agreement between the predictions of the EMT for the binding energies of the excited states and experiment is excellent, with the theoretical predictions in agreement to better than 0.01 meV with the experiment. This result manifests that we have an excellent theoretical understanding and knowledge of the electronic states and their effective masses at the bottom of the conduction bands in Ge (or Si where a similar situation exists). Theoretical effort has also been devoted in order to predict the binding energy, chemical split and shifts of the donor GS which, as previously mentioned, are beyond the framework of the EMT, from different approaches which try to take into account the changes in energy by the introduction of a specific type of impurity atom in the lattice. Due to the difficulty of this approach, it is worth mentioning that some very good GS energies have been calculated for the As donor in Ge and the P donor in Si [28]. Fig. 3 summarizes the GS binding energies of the donors known in Ge.

2.2. The degeneracy and symmetry nature of donor levels

Two techniques have been used in solid state spectrocopy to study and determine the degeneracy of impurity states in solid state spectroscopy: the Zeeman effect by means of the application of magnetic fields and the application of uniaxial stress fields. The Zeeman effect breaks the Kramers degeneracy, $(m, -m)$, and displays the multivalley degeneracy of the excited states due to the different projections of the

H-field along the present non equivalent electron conduction band minima which have, by necessity, different alignments with respect to the field.

The uniaxial stress fields break the degeneracy due to the site group symmetry, which is some subgroup of the cubic symmetry group for the Ge and Si lattices, by a combination of reducing the actual symmetry under the application of a preferential symmetry axis [29], along the applied field, and the coupling of the donor states to the elastic deformation potential introduced by this field [17]. By the same process as in the Zeeman effect, the multivalley degeneracy is also broken and different valleys couple with the different projected strengths along their constant energy ellipsoid axes. Additionally, in stress experiments where the stress field is aligned along one of the [111] directions in Ge (or [100] in Si), the corresponding conduction band minimum is lowered in energy with respect to the other three and the zero stress energy. The other three minima in turn increase in energy respect to the zero field value, following almost a parallel response to taht of the excited states *if they belong to irreducible representations of the symmetry group* T_d [30]. This fact and the number of levels in which the excited states split under the application of the uniaxial stress are axploited to establish spectroscopically the site symmetry *i.e.* that of the Hamiltonian that reflects on the excited states of the donor.

In this paper we will review the Zeeman effect experiments performed on the donor D(H, O) in ultrapure Ge [31] and their theoretical interpretation [31,32]. The Zeeman experiments on this donor in ultrapure Ge are of particular interest because of the extreme sharpness of its transitions. This allowed spectral resolution of the split components of the bound excited states sequence $2P_{\pm}$, $3P_{\pm}$, $4P_{\pm}$, $4F_{\pm}$, $5P_{\pm}$, $5F_{\pm}$ and $6P_{\pm}$ (as usual in this field, we follow Faulkner's labels for the sequence of observed transitions) at magnetic field values as low as 0.5 KOe (500 Gauss) [31]. This is by far the largest sequence of excited state splittings observed for donors is semiconductor physics.

The Zeeman study of the D(H, O) donor in Ge is of additional interest due to the observation that nuclear motion of the hydrogen atom around the four equivalent tetrahedral positions (ETP) with respect to the O-Ge bonds affects the GS energy [20]. This fact manifests itself in some different characteristics for the $1S$ manifold of the D(H, O) as compared with that of a elemental substitutional donor as As, Sb or P. The $1S$ manifold is expected to consist of a total of 4(ETP) × 4(valleys) = 16 states [20] grouped in five levels, with three of them experimentally observed [21] compared to 4 states grouped in two levels for the elemental donors [11].

2.2.1. The Zeeman effect of donors in Ge. Experiments: Figure 4 presents the Zeeman or "fan" diagram that summarizes the resultant magnetic field dependence of the energy positions of the observed transitions of the D(II, O) donor in Ge. This diagram shows the wealth of splittings that have been resolved. It is also clear in Fig. 4 how each pair of partner transitions $nP_{\pm}$ split asymmetrically with respect to the zero-field energy positions, a result different from what is observed in one-electron atomic levels, where the Zeeman split for these low fields is far more symmetric. The diagram also shows a fourfold split for each transition instead of the expected two from the $(m, -m)$ pair. One pair of these four split transitions

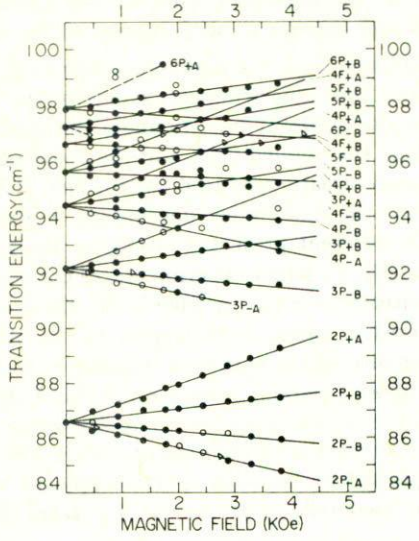

FIGURE 4. Zeeman response of the observed transitions between electronic states of the D(H, O) donor in Ge. At the right hand side the final quantum state of the transition is indicated, from Ref. [31].

are labeled as $nP_{\pm A}$ and the other pair as $nP_{\pm B}$. The labels A, B correspond to the H-field being applied parallel to one of the [111] crystallographic axes, *i.e.*, parallel to one of the conduction band minima major ellipsoid axis, A-valley, and forming an angle $\cos^{-1}(1/3)$ with respect to their major ellipsoid axes for the other three conduction band minima; B-valleys. As a consequence, the appearance of the extra two-fold spliting of the B-valleys is just the normal excited donor state Zeeman splitting expected for a field strength of $H/3$.

Figure 5 shows a superposition of line positions as a function of field for energy differences from the zero field $2P_{\pm}$ energy position of the D(H, O) [31], P [31], Sb and As [33] donors. It can be seen that the magnetic response of the three donors is identical within experimental errors. This comparison allows to conclude that even though the D(H, O) has a $1S$ manifold very different from those of P and As, its actual 1S GS also does not exhibit a measurable magnetic field response [32,33,34].

2.2.2. Theory of the Zeeman effect of donor states in Ge. The EMT Hamiltonian of an electron bound to a donor center subjected to a magnetic field H along the z direction, defined by a vector potential $\mathbf{A} = \mathbf{H} \times \mathbf{r}/2$, can be written in cylindrical coordinates as

$$H = -\nabla^2 + (1-\beta)\frac{\partial^2}{\partial z^2} - i\gamma\frac{\partial}{\partial \phi} + \frac{1}{4}\gamma^2\rho^2 - \frac{2}{(\rho^2+z^2)} \tag{3}$$

where $\beta = m_t/m_l$, γ is the reduced field $\gamma = \hbar\omega_c/2R_y$ and $\omega_c = eH/m_t c$ is the

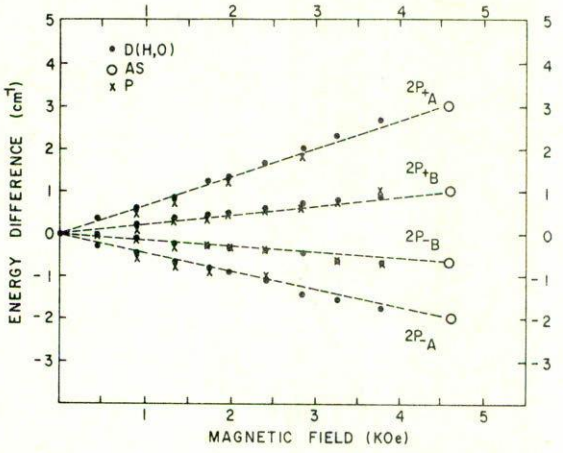

FIGURE 5. Comparison between the Zeeman response of the $2P_{\pm}$ transitions of the P, As and D(H, O) donors, Ref. [31].

transverse cyclotron frequency. The Hamiltonian (3) is written in the atomic units defined in Eq. (2).

The Hamiltonian (3) is invariant under rotations about the z axis and inversion. Therefore, the magnetic quantum number and parity are still constants of the motion and good quantum numbers for the eigenfunctions.

Under this theoretical framework it is expected that the energy difference between the two components of the Zeeman-split levels (corresponding to states with opposite signs for m) is

$$\Delta E = E_{n,+m} - E_{n,-m} = 2m\gamma = \frac{mh}{m_t R_y c} \begin{cases} H & A \text{ valley}, \\ H/3 & B \text{ valley}. \end{cases} \tag{4}$$

Figure 6 shows the observed split energies ΔE for the A valleys GS to $2P_{\pm}$, $3P_{\pm}$ and $4P_{\pm}$ levels transitions compared with the theoretical prediction represented by the steeper solid line. The observed agreement is excellent. There are some systematic deviations for the case of the B valley transitions due to the fact that the projection of the field along the minor ellipsoid axis of the CB constant electron energy surfaces that affect the electrons with longitudinal masses has been neglected in the Hamiltonian (3) [31].

2.2.3. Solution of the Donor Hamiltonian in a magnetic field. Taking advantage of the invariance of the Hamiltonian under rotations about the z axis and of the fact that parity is also a good quantum number, the eigenfunctions can be written as [32,33,34]

$$F_{n,m}(\mathbf{r}) = f_{n,m}(\rho, z)e^{im\phi} \tag{5}$$

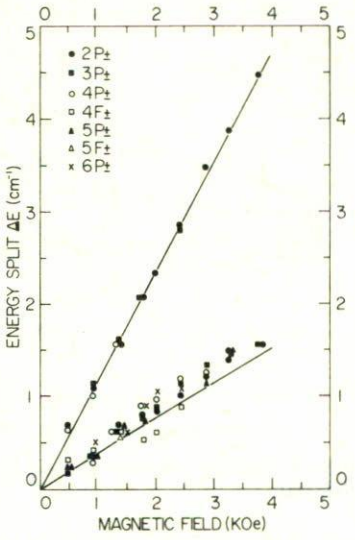

FIGURE 6. Split cyclotron Zeeman energies for D(H, O) donor states associated to the minima of the A and B valleys, Ref. [31].

where n represents the set of additional quantum numbers associated with any other constants of motion of the Hamiltonian.

In Eq. (4) one can calculate that $\gamma = 1$ for a magnetic field of 61.6 KOe. The fields used in the Zeeman experiments on the D(H, O), are $0 \leq \gamma \leq 0.08$, *i.e.*, it is a low field region problem.

Nisida and Horii [33] (NH) examined the eigenvalues of the donor magnetic Hamiltonian Eq. (3) for the $1S$, $2P_0$, $2P_\pm$ and $3P_\pm$ states. They compared the calculated energy eigenvalues obtained by using hydrogenic variational and harmonic oscillator-like WF's. They found for the $1S$ and $2P_0$ states that the hydrogenic wavefunctions (HWF) provide smaller energies than the harmonic oscillator WF's (HOWF) for $\gamma \leq 0.7$. As a variational calculation always provide only an upper bound to the real eigenenergy it is necessary to take the lowest calculated values as the best approximations. For the $2P_-$ state this γ range reduces to $\gamma \leq 0.15$. From these results they deduced that the HOWF should give better energy results for higher energy excited states, and their calculations of the $3P_-$ state were done entirely using HOWF.

NH's main interest was fitting observations of the Zeeman effect of As and Sb donors [34] at fields H larger than 5 KOe, *i.e.*, for $\gamma \geq 0.08$, the complementary region to that examined by Navarro *et al.* [31] for the P and D(H, O) donors. Hence, the published results of NH are very difficult to use for the $\gamma \leq 0.08$ region.

For this reason, in order to compare the Zeeman results for the D(H, O) at the small fields applied with the theoretical predictions, we had to recalculate the energy response of the donor levels $1S$, $2P_\pm$, $3P_\pm$ and to extend it to the $4P_\pm$ state, whose magnetic splitting was quite clearly observed for the D(H, O) [32]. The variational

calculations were performed using both HWF and HOWF, and choosing the set of smaller resulting energies.

In Table II, the analytical expressions for the HWF and HOWF are shown. The WF's were orthonormalized prior to the variational minimization procedure of the pair of parameters (a, b) for each $F_{n,m}(\mathbf{r})$. In Table III, the expressions for the variational energies calculated for each state (n, m) under both sets of WF's HWF and HOWF are shown, as calculated from the general expression

$$E = (F, HF) = E_0 + \int F_i^*(\mathbf{r}) \left(m\gamma + \frac{\alpha^2 \rho^2}{4} \right) F_i^*(\mathbf{r})\, dV \tag{6}$$

where the F_i is each one of the variational functions in Table II, and E_0 is the zero-field energy state.

In Figure 7 the calculated energy values are shown for both, the HWF curves (I), and the HOWF curves (II). In this diagram the energies are expressed in terms of the negative Ge donor Rydberg $E_y = -4.35$ meV. It can be seen in the diagram that for the $3P_+$ state the HWF energy values are better only for $\gamma \leq 0.013$ (0.8 KOe) and for higher fields the HOWF provide lower energies. For the $4P_\pm$ state the HOWF provide better energy values right from the zero-field value. For the $1S$ and $2P_\pm$ state following NH [33], HWF were used for the entire range of magnetic fields used ($\gamma \leq 0.08$).

The magnetic field dependent transition energies calculated for the $1S$ to $2P_\pm$, $3P_\pm$ and $4P_\pm$ are shown in Figure 8, compared with the observed energies. The fit is very good for most of the field values, with just one very small discrepancy for the $1S$ to $4P_{-A}$ transition at 4 KOe that lies close in energy to a line identified as $3P_{+B}$. The most striking result is how naturally the theory predicts the strong asymmetric energy splittings around the zero-field energy positions, without the use of fit parameters.

An important result is that the transitions labeled $4P_\pm$ were fitted asumming a $P_\pm$ character. A similar calculation is pending to check for the proposed $4F_\pm$ character by BCV [16] for this transition, although from the fan diagram for the Zeeman effect on all these transitions (Fig. 4), only small differences are observed in the Zeeman response at the low applied fields for the two transitions labeled $4P_\pm$, $4F_\pm$, so that one would expect also virtually insignificant differences to result from the theory.

One can conclude from our theoretical analysis of the Zeeman effect of donor transitions in Ge that we have a good theoretical understanding of the donor dynamics and quantum nature of its electronic states, reinforcing the conclusions obtained from the excellent agreement between the zero-field bound state energies predicted and observed, as discussed above.

2.3. The photoionization and electron capture cross sections

2.3.a. The donor photoionization cross sections. The problem of the photoionization cross section of an electron in a donor state can be approached by resorting to

Donor State	Hydrogen-like wave function (HWF)	Harmonic oscillator-type wave function (HOWF)
$1S$	$\frac{1}{(\pi a^2 b)^{1/2}} \exp - \left[\frac{\rho^2}{a^2} + \frac{z^2}{b^2}\right]^{1/2}$	$\frac{1}{(8\pi^3 b^2)^{1/4} a} \exp - \left[\frac{\rho^2}{4a^2} + \frac{z^2}{4b^2}\right]$
$2p_0$	$\frac{1}{(\pi a^2 b^2)^{1/2}} z \exp - \left[\frac{\rho^2}{a^2} + \frac{z^2}{b^2}\right]^{1/2}$	$\frac{1}{(2\pi b^2)^{3/4} a} z \exp - \left[\frac{\rho^2}{4a^2} + \frac{z^2}{4b^2}\right]$
$2p_\pm$	$\frac{1}{(\pi a^4 b)^{1/2}} \rho \exp - \left[\frac{\rho^2}{a^2} + \frac{z^2}{b^2}\right]^{1/2} e^{\pm i\phi}$	$\frac{1}{2a^2 (2\pi^9 b^2)^{1/4}} \exp - \left[\frac{\rho^2}{4a^2} + \frac{z^2}{4b^2}\right] e^{\pm i\phi}$
$3p_\pm$	$\frac{2^{1/2}}{(5\pi a^2 b)^{1/2}} \left[\frac{-5}{2} + \left[\frac{\rho^2}{a^2} + \frac{z^2}{b^2}\right]^{1/2}\right] \rho \exp - \left[\frac{\rho^2}{a^2} + \frac{z^2}{b^2}\right]^{1/2} e^{\pm i\phi}$: (HWF)	
		(HOWF): $\frac{1}{2^{1/4}\pi^{3/2}(8a^4 b)^{1/2}} \left(1 - \frac{1}{b^2} z^2\right) \rho \exp - \left[\frac{\rho^2}{4a^2} + \frac{z^2}{4b^2}\right] e^{\pm i\phi}$
$4p_\pm$	$\frac{2^{1/2}}{(15\pi a^4 b)^{1/2}} \left[\frac{15}{2} - 6\left[\frac{\rho^2}{a^2} + \frac{z^2}{b^2}\right]^{1/2} + \left[\frac{\rho^2}{a^2} + \frac{z^2}{b^2}\right]\right] \rho \exp - \left[\frac{\rho^2}{a^2} + \frac{z^2}{b^2}\right]^{1/2} e^{\pm i\phi}$: (HWF)	
		(HOWF): $\frac{1}{2^{1/4}\pi^{3/2}(7a^4 b^3)^{1/2}} \left(z - \frac{z^3}{2b^2}\right) \rho \exp - \left[\frac{\rho^2}{4a^2} + \frac{z^2}{4b^2}\right] e^{\pm i\phi}$

TABLE II. Trial wave functions with variational parameters a, b, different for each donor state.

Donor State	Calculated with HWF	Calculated with HOWF
$1s$	$\epsilon = \epsilon_0 + m\gamma + \frac{\gamma^2 a^2}{4}$	
$2p$	$\epsilon = \epsilon_0 + m\gamma + \frac{3\gamma^2 a^2}{4}$	
$2p_\pm$	$\epsilon = \epsilon_0 + m\gamma + \frac{3\gamma^2 a^2}{2}$	
$3p_\pm$	$\epsilon = \epsilon_0 + m\gamma + 3.3\gamma^2 a^2$	$\epsilon = \epsilon_0 + m\gamma + \gamma^2 a^2$
$4p_\pm$	$\epsilon = \epsilon_0 + m\gamma + 5.7\gamma^2 a^2$	$\epsilon = \epsilon_0 + m\gamma + \gamma^2 a^2$

Note: $\epsilon_0 = \epsilon_0(a, b)$ is the same mathematical expression calculated for the state energy at zero field, in terms of a, b [32].

TABLE III. Mathematical expressions of the variational energies to minimize, of donor states in a reduced magnetic field $\gamma = \frac{H(\text{KOe})}{61.6}$, in Donor Rydberg Units, see text.

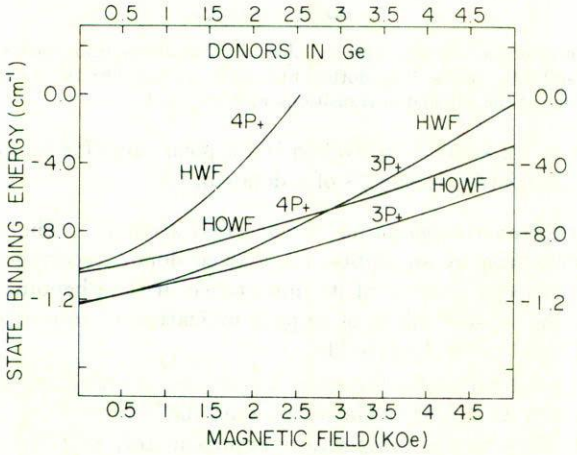

FIGURE 7. Zeeman response calculated for the $3P_{+A}$ and $4P_{+A}$ states. HWF stands for hydrogen-like wavefunction and HOWF stands for harmonic oscillator-like wave function.

the analogous problem of the photoionization of the electron in the hydrogen atom and trying to adapt the expressions derived in this case. However, it is simpler to use the IR absorption spectra at a given value of the donor concentration and use the simple formula

$$\alpha(\lambda) = N_d \sigma_{1s}(\lambda) \tag{7}$$

where α is the absorption coefficient at the λ wavelength, N_d is the concentration of noncompensated donors, and $\sigma_{1s}(\lambda)$ is the photoionization cross section. In this way one can calculate that for the Sb donor in Ge from the published spectra [24]

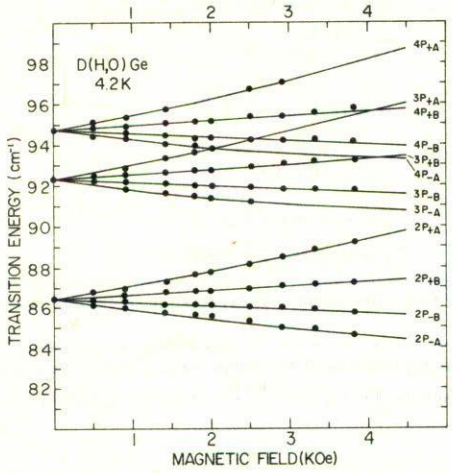

FIGURE 8. Zeeman response calculated for the observed transitions from the GS to the split $2P_{\pm}$, $3P_{pm}$ and $4P_{\pm}$ states. The dotted lines help to visualize the deviation from linear behaviour of the calculated transitions with the field.

σ_{1s} ($\lambda = 98$ μm) $= 1.2 \times 10^{-14}$ cm^2 which is a typical value for the photoionization cross section of an electron in the GS of a donor in Ge.

2.3.b. The electron recombination donor cross section. The problem of the recapture of an electron by an empty, *i.e.* ionized donor, received early attention in semiconductor theory because of its importance in the phenomena of electrical breakdown and the related effect of impact ionization of impurities by electron avalanches discovered in 1953 in Ge [35].

The experimental values for the cross sections for electron recombination with the donor impurities As and Sb in Ge are between 10^{-11} to 10^{-14} cm^2 for T between 4 and 10 K [36]. They vary in temperature approximately as $T^{-2.5}$.

The following are competing possible recombination mechanisms: the conduction electron may make a transition to the ground state of the donor accompanied by either emission of 1) light or 2) a phonon, or 3) it may be captured by an excited state with a subsequent cascade of transition processes by means of which the electron falls down to the GS. These transitions are 10^4 to 10^5 times faster [22] when they are accompanied with the emission of acoustic phonons rather than light.

The cross section for direct recombination with emission of light is obtained by using the well known result for the radiative recombination of an electron with a proton to form hydrogen making the appropiate substitutions for the spherical effective conduction electron mass and the Ge dielectric constant for the coulombian interaction. At 4 K the corresponding recombination cross section results in [37] $\sigma \cong 4.2 \times 10^{-19}$ cm^2, *i.e.*, seven to eight orders of magnitude smaller the observed one.

If direct recombination with emission of a phonon is regarded as the main alternative mechanism responsible for the removal of electrons from the CB, N. Lax [38]

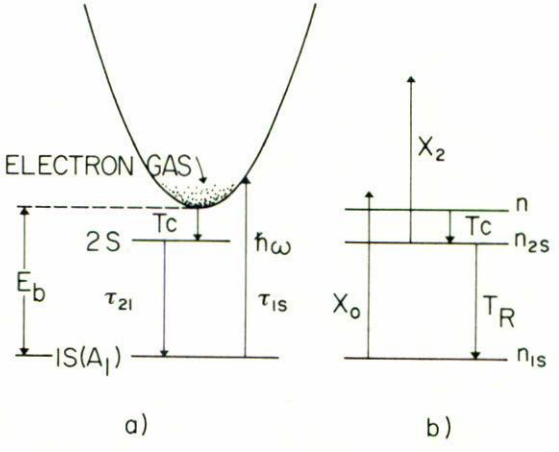

FIGURE 9. Three level model for free electron recapture by a donor in Ge. a) parabolic band picture, b) schematic picture.

calculated the cross section as

$$\sigma = \frac{256\pi\Xi^2\hbar^5 c_s^3}{\rho a^{*6} E_i^5 kT} \tag{8}$$

where Ξ is the deformation potential constant (=16 eV), c_s the longitudinal sound velocity in Ge ($= 5.4 \times 10^5$ cm/sec), ρ the density of Ge, k the Boltzmann constant and E_i is the donor ionization energy taken as 10 meV for the purpose of estimating this cross section. At 4 K this cross section is $\sigma = 5 \times 10^{-15}$ cm^2, again too small to account for the observed values.

The model for the recombination consisting of the capture of an electron by some highly excited, donor state and the subsequent transition to a lower lying state to finally arrive to the GS by means of acoustic phonon emissions, Fig. 9a, provides satisfactory explanations for the observed magnitudes and temperature dependence of these cross sections. As the photoionization cross sections for the excited states are much smaller than that of the FS, once an electron is captured, it inevitably returns to the GS.

The theory for this type of process was developed in a series of papers by the following authors: Lax [38], Ascarelli and Rodríguez (AR) [37], and Brown and Rodríguez (BR) [39]. The essential physical details of the model after AR are the following: The total recombination cross section is given by

$$\sigma = \sum_j \sigma_c(j) S_j \tag{9}$$

here, $\sigma_c(j)$ is the electron capture cross section of the j-th donor state deduced by

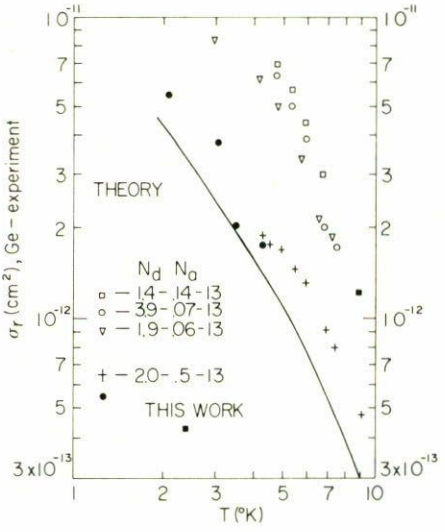

FIGURE 10. Summary of measured electron-ionized donor cross sections in Ge. The numbers that indicate the donor and acceptor concentrations are given in 10^{-14} cm^{-3}, Refs. [36] and [37].

AR to be

$$\sigma_c = \frac{g_j \pi^2 h \beta_j^2}{2m^*(kT)^2} \exp(E_j/kT) \tag{10}$$

here g_j is the degeneracy of the j-th level, E_j its energy, and β_j is the probability per unit time for thermal ionization of an electron from this state. S_j is the probability that an electron bound in this level will not be ionized into the CB. Sometimes this probability is called the "sticking" probability of the level. From formula (9) it is inferred that those levels with both large sticking probabilities and capture cross sections give the largest contributions to the total recombination cross section.

AR calculated the probabilities per unit time that the electrons captured in a state j will make a transition to some lower lying state j' with the simultaneous emission of an acoustic phonon using the well known Frohlich Hamiltonian [40] for the electron-phonon interaction. Their results, as well those of BR, show that by large factors the largest contributions arise from capture in the $2S$ and $3S$ levels with subsequent transition to the GS with emission of one acoustic phonon. Capture by the state $2S$ contributes to a factor of ten times more than that from the 3S [37].

In Fig. 10 is shown a compilation of experimental data [36] for the recombination cross section of electrons in As and Sb donors in Ge including the value at 9 K obtained in this work and a comparison with the theoretical calculations of AR. It can be seen that the AR results give a very satisfactory concordance with observed data at $T \leq 4$ K, and a good estimate for the rest of the experimental values. Although

the theory of AR is somewhat old, it is certain that it incorporates the true physical agents that determine the recombination cross sections of conductions electrons into donor centers. One improvement could come from using more adequate WF's instead of the hydrogen WF's used.

In the next section, we describe some experimental results that provide a more recent experimental estimate for σ_c of Sb donors in Ge at $T = 9$ K and agree very well with the extrapolation to this temperature of the early experimental results of Koenig *et al.* [36].

2.4 The saturation of the absorption of radiation by donors

In a recent work, Theiler *et al.* [41,42] have observed in a series of photoconductive experiments on the D(H, O) donor ($\epsilon_i = 12.498$ meV) with above but near the ionization edge radiation of $\lambda = 90.09$ μm ($h\nu = 13.67$ meV, or 111 cm^{-1}) at high excitation powers a total bleaching of the electrons in the GS of this donor, taking < 1 μsec for its population to be fully recovered [42].

These phenomena require for its understanding a knowledge of the donor-electron recombination parameters in Ge. [36,43] In particular McManus *et. al.* 43 report a study on the nonlinear absorption of infrared radiation of $\lambda = 10.6$ μm, ($h\nu = 116.97$ meV) by Sb donors in Ge. *i.e.* for radiation more than eleven times their ionization energy. In these experiments it is required that in order for the electrons to come down to the bottom of the conduction band previous to their recapture by the donor centers, they have to shed away the excess energy by means of successive emissions of optical and acoustic phonons [44], a process which heats the distribution of electrons in the conduction band to some T_e significatively different from that of the lattice [44]. This fact affects among other parameters the donor capture cross section of electrons, as it is discussed in the present work.

We review here a study [45] of the saturation of the absorption coefficient of P ($\epsilon_i = 12.88$ meV) and Sb ($\epsilon_i = 10.45$ meV) [17] donors in n-type Ge ($N_d \approx 10^{15}$) when subjected to high power pulses of near ionization edge radiation $\lambda = 90.09$ μm (111 cm^{-1}), as model systems to study the kinetic process that governs the recapture of electrons by the D(H, O) donor center under analogous conditions, and to obtain the physical parameters that regulate the recombination of electrons promoted close to the bottom of the CB. This is possible because the D(H, O) donor complex, as well as P, Sb and any other donor in Ge, according to the effective mass theory model (EMT) have identical sets of excited states, both in their energy spacings and WF nature, [12] and we have discussed in the last section how the electrons in the CB return through donor excited states to the GS [37].

In Fig. 11 a plot of the dependence of the absorption coefficient on the relative laser intensity of $\lambda = 90.09$ μm is shown. 0 dB correspond to a peak intensity of 22.6 KW/cm^2 and pulse energy of 0.77 mJ. The non-linear change of the absorption takes three to four decades of increasing laser intensity. This result is similar to that observed for absorption at $\lambda = 10.6$ μm [43]. So, what is measured is the saturation change not of the true absorption coefficient $\alpha(\lambda, I)$ but that of the average absorption coefficient $\overline{\alpha(\lambda, I)}$ resulting from the convolution of $\alpha(\lambda, I)$ with

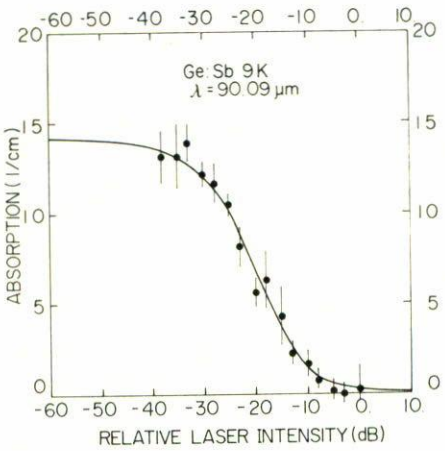

FIGURE 11. Observed saturation effects of the absorption coefficient at $\lambda = 90.09\ \mu m$ ($111\ cm^{-1}$) of Sb and P donors.

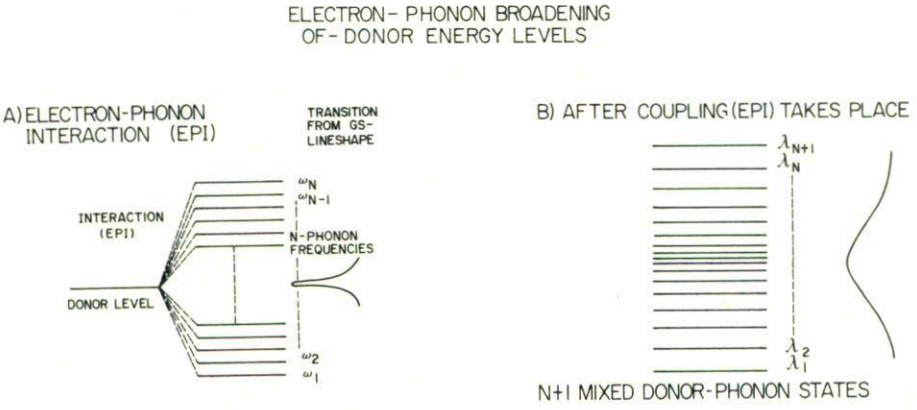

FIGURE 12. a) Thermal phonon field broadening for donor levels, b) the phonon background couples with the donor levels resulting in a broader envelope of all these levels.

the laser pulse intensity distribution in space and time. The solid line represents the fit of the three-level model discussed below [43]. In contrast to the observed results of the absorption saturation at $\lambda = 10.6\ \mu m$, where the electrons are pumped way above the CB, for the results in Fig. 11, the case for $\lambda = 90.09\ \mu m$, and the electrons pumped just above the bottom of CB, the theoretical fit is very satisfactory, using natural parameters of Ge.

2.4.1 Discussion. The essential process and levels involved in the kinetics of the photoionization and recombination of electrons by a donor in Ge are illustrated

schematically in Fig. 12a. The recombination of an electron by a donor proceeds through its capture by some excited state and subsequent cascading by acoustic phonon emission to the GS. As discussed in the last section, the calculation of AR [37] show that by large factors the most important contribution to the electron capture cross section σ_c arises from capture into the level $2S$ with subsequent transition to the GS with emission of one acoustic phonon. Hence, in Fig. 9 only the effects on the kinetics due to the capture by the $2S$ level have been depicted. Once an electron is trapped by some donor excited level it will come down, in most cases to the ground state due to the fact that the photoionization cross sections of the excited states are several orders of magnitude smaller than that of the GS [37].

2.4.2 Results. In Fig. 9a, no account has been taken of the fact that donors in Ge have the four possible $1S$ states, originating in the four degenerate CB minima, chemically split into two levels, a singlet $1S(A_1)$ and a triplet $1S(T_2)$. The reason is that the recombination lifetime τ_{11} from $1S(T_2)$ to $1S(A_1)$ is at least one order of magnitude smaller than that of the recombination time τ_{21} from the $2S$ to $1S(T_2)$, which is the bottleneck in electron recombination, *i.e.* 10^{-10} sec. [37,43] The recombination lifetime τ_{32} from $3S$ to $2S$, is expected to be of the same magnitude as τ_{11} [37,43].

If the photoionization time τ_{1s} is comparable or smaller than the recombination lifetime of an excited level there can be an electron population buildup in this state. As the photoionization time $\tau_{1s} = (\sigma_{1s}\Phi)^{-1}$, where σ_{1s} is the GS photoionization cross section $\sigma_{1s} = 1.2 \times 10^{-14}$ cm^2, and Φ is the photon flux 4.54×10^{20} photons-cm^{-2}/Watt-sec for $\lambda = 90.09$ μm, one gets $\tau_{1s} \approx 10^{-9}$ sec. at the incident power of -23 dB in Fig. 11 and above it. As a consequence, the $2S$ state will have an appreciable effect on the overall absorption process because τ_{21} has been calculated [48] as 2×10^{-9} sec. *i.e.*, for most of the powers for which non-linear absorption is observed. This effect is reinforced by the fact that its photoionization cross section is at least one order of magnitude smaller [49] than that for the $1S$ electrons. Hence, the kinetics is best described by a model involving the three intervening levels, the GS, the CB, and the $2S$ state.

The power dependent $\alpha(\Phi)$ absorption coefficient expression that applies for the three level situation described above has been deduced from the corresponding rate equation in the literature [42,43] using the model illustrated in Fig. 9b with $X_0 = 1/\tau_{1s}$, $T_c = \sigma_c(N_A + n(\Phi))$, $T_R = 1/\tau_{21}$, as follows,

$$\alpha(\Phi) = n_{1s}(\Phi)\sigma_{1s} + n(\Phi)\sigma_f \tag{11}$$

where n_{1s} and n, are the number of electrons in the donor GS, ionized into the CB and given from the steady state solutions of

$$\frac{dn_{1s}}{dt} = -X_0 n_{1s} + T_R n_{2s}, \tag{12}$$

$$\frac{dn_{2s}}{dt} = T_c n(\Phi) - T_R n_{2s} - X_2 n_{2s}, \tag{13}$$

$$\frac{dn}{dt} = X_0 n_{1s} - T_c n(\Phi) + X_2 n_{2s}, \tag{14}$$

$$N_D - N_A = n_{1s} + n_{2s} + n(\Phi). \tag{15}$$

Solving these equations for $n(x)$ and n_{1s} we obtain immediately for $\alpha(x)$ given by Eq. (11),

$$\alpha(x) = \frac{1}{1+Bx}\left[\alpha_0 - \frac{1}{2}\left[\frac{\alpha_0}{1+Bx} - \alpha_\infty\right]\left[-x + (x^2 + 4x(1+Bx))^{1/2}\right]\right] \tag{16}$$

for negligible donor compensation and free carrier absorption cross section σ_f, and

$$x = \frac{\sigma_{1s}\Phi(1-R)}{N_d \sigma_c \langle v\rangle}, \qquad B = N_d \sigma_c \langle v\rangle \tau_{21} \tag{17}$$

where $R \cong 0.3$ is the reflectivity of the sample, N_d is the donor concentration, σ_c is the electron capture cross section, $\langle v\rangle$ is the thermal average free electron velocity $\langle v\rangle = 4.2 \times 10^6$ cm/s at $T = 9$ K, ($m_e^* = 0.220$), and α_0, α_∞ are the absorption coefficients at zero and very high laser power intensities, respectively. They are defined as

$$\sigma_0 = N_d \sigma_{1s}, \qquad \sigma_\infty = N_d \sigma_f. \tag{18}$$

The value of $\alpha_0 = 14.2$ cm^{-1} is obtained from the FIR transmission measurement and from it $\sigma_{1s} = 1.2 \times 10^{-14}$ cm^2 at $\lambda = 90.09$ μm. Several estimates exist done at the beginning of the sixties for the value of the electron capture cross section σ_c, mainly deduced from conductivity measurements. [36,37] However, there is a spread of published values that put its actual magnitude somewhere between 10^{-14} to 10^{-12} cm^2 for $T = 9$ K. Hence, σ_c together with τ_{21} are the only not well-known parameters in Eqs. (11–18). As a consequence, they were used as fitting parameters. The solid line represents the best fit given by Eq. (15), $\sigma_c = (1.4 \pm 0.3) \times 10^{-12}$ cm^2 and $\tau_{21} = (5.1 \pm 1.0) \times 10^{-10}$ sec.

The theoretical fit of the three level model provides a very satisfactory explanation of the observed saturation of the absorption coefficient of radiation with wavelength $\lambda = 90.09$ μm, a result that contrast to the case for $\lambda = 10.6$ μm for the same donor system [43]. The resulting value of the σ_c donor at $T = 9$ K is felt to be a very reasonable physical result. It comes very close in magnitude to the linear extrapolated value from the experimental results for σ_c of Sb donors measured by Koening *et al.* [36] of 1.1×10^{-12} cm^{-2}. The close agreement between these two different ways to estimate σ_c at 9 K is interpreted by us to imply that these represent the most realistic values for this parameter of the donors in Ge. The result for τ_{21} of half a nanosec. comes close to the above mentioned theoretical value of 2 nanosec [48]. Finally, the close agreement between the estimated capture cross sections of Koening *et al.* [36] and that calculated in this work using the average

thermal electron velocity at 9 K indicates negligible heating of the electrons promoted so close to the bottom of the conduction band, a result that should also hold for the saturation experiments at the same wavelength on the D(H, O) donor [42].

2.5 The transition linewidths. The coupling of donor states to the phonon background

The absorption lines corresponding to photon induced transitions of electrons in donor (or of holes in acceptors) have linewidths (full width at half maximum of FWHM) which typically do not reflect intrinsic properties of the isolated impurity in the crystal [22]. Scaling the matrix element for the dipolar transition between the $1S$ and $2P$ states of the H-atom to the physical dimensions of a donor in Ge and energy separation between these two levels one obtaines an expected FWHM of 2.7×10^{-5} μeV (2.7×10^{-11} eV). However, under ordinary circumstances observed FWHM of donor transitions in Si or Ge are of the order of 50–100 μeV.

The line broadening of transitions between shallow impurity states in Ge (and Si) was studied almost at the same time that absorption spectroscopy in the FIR between these states was initiated [51]. The dependence on impurity concentration and on temperature of boron lines in Si was studied by White [52]. The concentration dependence of the Sb donor in Ge was studied by Nisida and Horii [53]. The electric field Stark broadening of impurities in Ge was studied by Ohyama [54]. All these experiments were performed with electrically active impurity concentrations larger than 10^{13} cm^{-3} and were not free of stress and concentration broadenings with the best estimates for the FWHM $\simeq$ 50 μeV for these transitions. Jagannath *et al.* [55] on P in Si, doped by a neutron transmutation process, reduced substantially these effects to measure FWHM as small as $\simeq$ 25 μeV. However, the P donor is stress dependent in its transition linewidths and hence it is not possible to take this FWHM value as its intrinsic limit.

The stress dependence of impurity transition linewidths can be overcome by studying the absorption spectrum of one of the stress insensitive donors or acceptors in Ge [3]. A FWHM study on the donor D(H, O), which is stress insensitive in its linewidths and in ultrapure Ge to avoid concentration broadening has already been performed [22]. That work provides FWHM values of stress-free and impurity concentration-free transitions, as well as free of Stark broadening as the authors show in the paper. In this work we will review briefly the essential elements of that study for its importance to the donor spectroscopy.

2.5.1 Physical agents that affect the linewidths of donors. For atomic transitions of free atoms in a gas three factors affect the linewdith: [56] *i)* the radiative recombination FWHM, *ii)* the Doppler effect caused by the thermal distribution of velocities in the gas, and *iii)* a pressure dependent contribution originating grom collisions between atoms. The Doppler and collision broadenings contribute to the FWHM with factors proportional to $T^{1/2}$, T being the gas temperature, with an additional multiplicative dependence on the gas density for the collision processes. The radiative recombination lifetime FWHM is determined by the spontaneous emis-

sion rate (Einstein A coefficient [56]) and depends on the third power of the energy separation between the two transition levels as well as on the square of the absolute value of the matrix transition element D, *i.e.*, $1/\tau \simeq \Delta E^3 |D|^2$.

The quantum theory of the electromagnetic field and its interaction with matter tell us that in the presence of a thermal radiation field, the atomic levels, couple with the radiation field modes to produce a system of mixed states: atomic levels-radiation field modes. As a result of this coupling, the absorption FWHM show an extra broadening originating in the envelope of the multiplet of mixed states of varying intensities that replace the original atomic level. Many body theory and quantum theory provide the following result for this broadening in a radiation field at temperature close to the absolute zero [56]

$$\gamma_i(\omega) = \sum_{\omega<\omega_j} \gamma_{ij}(\omega), \tag{19}$$

where

$$\gamma_{ij}(\omega) = \frac{e^2|D_{ij}|^2}{6\pi\epsilon_0 hc^3}(\omega - \omega_j)^3, \tag{20}$$

and D_{ij} is the electric dipole moment matrix element between the pair of states i and j. These two equations, (19) and (20), show how the actual FWHM has contributions of all possible electric dipole moment allowed transitions between the atomic level in consideration and those lower in energy. At temperatures different from zero, the sum has to be extended to the full spectrum of atomic levels and the individual contributions have to be multiplied by the absoption or emission of one photon factors $f(E)$ or $1 + f(E)$, for levels above or below the i states, where

$$f(E) = \frac{1}{\exp(E) - 1} \tag{21}$$

is the Bose-Einstein thermal distribution factor, with E equal to the energy difference of the two levels in consideration.

In analogy, donor transitions are subjected, among other contributing factors, to a very similar type of broadening, but coming from the *background of phonons* of the host crystalline lattice, Fig. 12a. The theoretical treatment of the broadening of donor (or acceptor) transitions produced by the coupling of the impurity levels with the background phonon field is dealt with in two articles by Barrie and Nishikawa (BN) [57,58]. The resulting broadening was found to be very similar to that of the atomic quantum level-radiation field coupling. In mathematical terms, the contribution to the broadening of a state i due to some lower lying energy state j is expressed as

$$\gamma_1 = \frac{\hbar R}{2\pi}|\Theta_{ij}(q)|^2(\omega_i - \omega_j)^3, \tag{22}$$

with

$$R = \frac{\Xi^2}{\rho \hbar a^2 v^3}. \tag{23}$$

The symbols used in Eqs. (22) and (23) are: v the velocity of longitudinal-acoustic phonons in Ge ($= 5.4 \times 10^5$ cm-sec^{-1}), a the Bohr radius, q the wavevector of the longitudinal-acoustic phonon with energy $(h(\omega_i - \omega_j)$, $\Theta_{ij}(q)$ the q-Fourier transform of the overlap of the envelope WF for the i and j states, ρ the Ge density ($=$ 5.32 g/cm), and Ξ the strength of the longitudinal-acoustic phonon-electron coupling in a donor level, *i.e.* it is the deformation potential constant for Ge ($=$ 16 eV). Again, it is necessary to multiply at finite temperatures by the phonon emission and absorption factors $1 + f(E)$ and $f(E)$, by levels below and above the i level, respectively.

BN discuss how for large energy differences between the i and j levels the overlap between the wave functions vanishes with high powers of the wave vector q, in such a way that the most important contributions come from the few lower levels closest to the i level [58]. Comparing Eqs. (21) and (23) for the atomic EM radiation coupling and for the donor levels' acoustic phonon broadening shows a striking formal similarity. The reason for this is, of course, the analogous physics of the two cases. The contribution to the FWHM of the $1S$–$2P_{\pm}$ transition due to the phonon coupling of the $2P_{\pm}$ level results in $\simeq$ 3–5 μeV for donors in Ge [22] figures that compare very favorable with the observed intrinsic linewidths of the transitions of the D(H, O) donor $\simeq$ 8 μeV, Fig. 13 [22]. The picture just discussed for the electron-phonon limiting mechanism of the FWHM of donors transitions in semiconductors should replace the previous picture presented in Ref. [22]. In that work, the observed contribution of the same coupling to the FWHM was inaccurately described as due to the lifetime in a excited state being limited by phonon assisted transitions to neighbouring donor states, *i.e.* resulting in an effective coupling of a excited state to all other bound states.

There are other physical agents that contribute to the linewidth of transition between donor states in a semiconductor. The expected contributions from these to the FWHM measured for the transitions of the D(H, O) donor are:

a) Residual strains. The presence of residual impurities, as well as dislocations in the crystal, produce a random distribution of strains which shifts the energy levels of the impurities. The main stress broadening in donors is chemically specific. It comes from the nonlinear response of the stress-split GS components [17]. In the ultrapure Ge used in Ref. [22] the largest concentrations of impurities are the electrically inactive impurities (EII), which are estimated to be in concentrations of 10^{14} cm^{-3}, three orders or magnitude above the electrically active ones, *i.e.*, those that originate donor or acceptor states. The estimated broadening of transitions of donors sensitive to stress, in this case is of the order of 1–10 μeV, as was indeed observed for the P-donor in the sample used. On the contrary, D(H, O) was observed to be unaffected by the random strains, as expected.

b) Electric field broadening. All ionized impurities produce randomly distributed electric fields which contribute to produce a local total electric field for each position

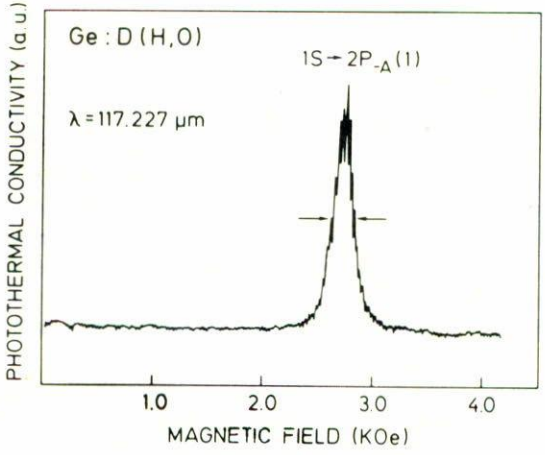

FIGURE 13. Observed linewidth for the $1S2P_{\pm}$ transition of the D(H, O) donor center in Ge. See text, Ref. [22].

Transition	Donor	FWHM
$1S \rightarrow 2P_{-A}$	D(H, O)	8.2 ± 0.4 μeV
$1S \rightarrow 3P_{-A}$		8.6
$1S \rightarrow 4P_{+A}$		7.2
$1S \rightarrow 4F_{+A}$		6.4 ± 0.2
$1S \rightarrow 2F_{-A}$	Phosphorous	26.6 ± 0.6

TABLE IV. Full width at half maximum intensity of the D(H, O) and phosphorous, single valley, donor transitions in ultrapure germanium as observed in Ref. [22].

in the crystal. Thus, again each transition line corresponds to a superposition of many individual lines shifted to different frequencies, producing what is called an inhomogeneously broadened line. This shift comes from the Stark effect on the donor levels. The Stark effect of impurity levels in Si or Ge has been extensively studied in the literature. [17,59,60] The theoretical Stark effect in this case has a maximum expected line broadening contribution of 1.4×10^{-2} μeV. Experimentally it was also possible to exclude any Stark effect broadening by the well known technique of measuring the absorption or photoconductivity with similtaneous illumination of the crystal with band gap light. [22] This has the effect to neutralize practically all acceptor or donor impurity states by means of the capture of the large number of electrons and holes created in the conduction and valence band by the illuminating radiation. Thus, in this situation all random electric fields are quenched.

c) Concentration broadening. At a certain impurity concentration, overlap of excited-state orbits becomes significant. The concentration at which this happens is $N_i \simeq 10^{13}$ cm^{-3} for the $3P$ state of a donor in Ge. [17,22,59] At the impurity concentrations used $N_i \simeq 10^{11}$ cm^{-3}, one estimates that up to states of main quantum number $n \geq 20$ no significant overlapping takes place.

In Table IV the FWHM measured for the donor transitions of D(H, O) and phosphorus are reported. Fig. 13 shows the obsrvation of the FWHM of the $1S$–$2P_{\pm}$ transition illustrating how through the magnetoabsorption this determination is performed. The abscissa is converted from difference in magnetic fields to difference in energies by means of the Zeeman slope of this transition as shown in Fig. 5. Table IV shows how the phosphorus $1S$–$2P_{\pm}$ transition is significantly stress broadened due to the presence of randomly distributed strains in the crystal.

Finally, from the experiment as well as from the BN theory it is possible to conclude that the determining physical process of the FWHM of the D(H, O) transitions originates from the coupling of the donor levels with the thermal phonon background. This phenomenon is illustrated in Fig. 12a,b. Using the relation $\tau = (\pi\Delta\omega)^{-1}$ results in $\tau = 0.16$ nsec for the electron lifetime in the $2P_-$ state.

Summary

We have reviewed the subject of the observation and theoretical understanding of the electronic states in donor impurities and donor complexes existing in germanium. We have discussed how the effective mass theory model provides a good theoretical framework to calculate and to explain the observed distribution of donor energy levels and their Zeeman response to small fields. The three level model used to explain the saturation of the absorption coefficient observed for ionization edge radiation of Sb-donors in Ge allows the determination of the decay time from the $2S$ to the $1S$ state ($\tau_{21} = 5.1 \times 10^{-11}$ sec.) and the electron-Sb donor recombination cross section at $T = 9$ K ($\sigma_c = 1.4 \times 10^{-12}$ cm^2). The physical agents that affect the linewidth of donor transitions were discussed. The observed intrinsic D(H, O) donor transitions' FWHM in the measurements of Navarro *et al.* [22], were reinterpreted as being determined by the envelope of the resultant coupled bound electron-phonon states due to the electron-acoustic phonon interaction at temperatures different from zero Kelvin.

Acknowledgements

Work partially supported by CONACYT (National Science and Technology Council of México) through Apoyos Especiales and DGICSA-SEP (Ministry of Public Education, México). One of us (H.N.), acknowledges the warm hospitality of the Max-Planck Institut at Stuttgart FRG, where most of the experimental work was done.

References

1. C. Winkler, *J.F. Praktische Chemie, Neue Folge* **34** (1986) 177.
2. E.E. Haller, *Mikrochim. Acta [Wien]* **III** (1987) 241. See also E.E. Haller, *Festkoerperprobleme*, XXVI, (1986) 203.
3. E.E. Haller, W.L. Hansen, and F.S. Goulding, *Adv. in Physics* **30** (1981) 93.

4. E.E. Haller and F.S. Goulding, *Handbook on Semiconductors*, Vol. 4, Ch. 6, 799. Edited by C. Hilsum, North-Holland, Amsterdam (1981).
5. C. Kittel, *Introduction to Solid State Physics*, Fifth edition, p. 232. John Wiley and Sons, New York (1976).
6. N.F. Mott and R.W. Gurney, *Electronic Precession in Ionic Crystals*, p. 166. Oxford University Pres, London (1940).
7. See also W. Kohn, "Shallow impurity states in Si and Ge", in The *Solid State Physics Series*, edited by F. Seitz and D. Turnbull, Vol. 5, p. 257 Acadmic Press, New York (1957).
8. R.J. Bell, *Introductory Fourier Transform Spectroscopy*. Academic Press, New York (1972).
9. Y. Tsunawaki, A. Yamanaka, and S. Kon, *Rev. Laser Eng.* **10** (1982) 78.
10. C. Kittel, and A.H. Mitchell, *Phys. Rev.* **96** (1954) 1488.
11. W. Kohn, and J.M. Luttinger, *Phys. Rev.* **97** (1955) 869.
12. R.A. Faulkner, *Phys. Rev.* **184** (1969) 713.
13. G. Dresselhaus, A.F. Kip, C. Kittel, *Phys. Rev.* **95** (1954) 568.
14. B.W. Levinger, and D.R. Frank, *J. Phys. Chem. Solids* **20** (1961) 281.
15. J.C. Ousset, J. Leontin, S.Askenazy, M.S. Skolnick, R.A. Stradling, *J. Phys. C* **9** (1976) 2803.
16. J. Broeckx, P. Clausws and J. Vennik, *J. Phys. C* **19** (1986) 511.
17. A.K. Ramdas and S. Rodríguez, *Rep. Prog. Phys.* **44** (1981) 1297.
18. N.O. Lipari and A. Baldereschk, *Solid State Commun.* **25** (1978) 665.
19. E.M. Gershenzon, G.N. Gol'tsman and A. Elant'ev, *Sov. Phys. JETP* **45** (1977) 555.
20. B. Joós, E.E. Haller and L.M. Falicov, *Phys. Rev. B* **29** (1980) 1907.
21. H. Navarro, J. Griffin and E.E. Haller, *Solid State Commun.*, **64** (1987) 1297.
22. H. Navarro, E.E. Haller and F. Keilmann, *Phys. Rev. B* **37** (1988) 10822, see also: E.E. Haller, H. Navarro and F. Keilmann, in *Proceedings of the 18th International Conference on the Physics of Semiconductors*, edited by O. Engstroem. World-Scientific, Singapore (1987), p. 837.
23. S.D. Secombe and D.M. Korn, *Solid State Commun.* **11** (1972) 1539.
24. J.H. Reuszer and P. Fisher, *Phys. Rev.* **135** (1964) A1125.
25. R.L. Aggarwal, P. Fisher, V. Mourzine and A.K. Ramdas, *Phys. Rev.* **138** (1965) A882.
26. E.E. Haller and L.M. Falicov, *Phys. Rev. Letters* **41** (1978) 1192.
27. P. Clauws and J. Vennik, *Phys. Rev. B* **30** (1984) 4837.
28. M. Altarelli, W.Y. Hsu and R.A. Sabatini, *J. Phys. C* **10** (1977) L605.
29. M. Tinkham, *Group Theory and Quantum Mechanics*. Mc Graw-Hill Inc., 1st. ed., p. 67, New York (1964).
30. H. Fritzsche, *Phys. Rev.* **125** (1962) 1560.
31. H. Navarro, J. Griffin and E.E. Haller, *J. Phys. C* **21** (1988) 1511.
32. M.A. Palomino-Ovando, M. Sc. Thesis, Puebla Univ. Unpublished (1988).
33. Y. Nisida and K. Horii, *J. Phys. Soc. Japan* **31** (1971) 776.
34. K. Horii and Y. Nisida, *J. Phys. Soc. Japan* **31** (1971) 783.
35. N. Sclar, E. Burstein, W.J. turner and J.W. Davisson, *Phys. Rev.* **91** (1953) 215.
36. S.H. Koenig, R.D. Brown and Walter Schillinger, *Phys. Rev.* **238** (1962) 1668.
37. G. Ascarelli and S. Rodríguez, *Phys. Rev.* **124** (1961) 1321.
38. H. Gummel and M. Lax, *Ann. Phys.* **2** (1957) 28, see also: M. Lax, *Phys. Rev.* **119** (1960) 1502.
39. R.A. Brown and S. Rodríguez, *Phys. Rev.* **153** (1967) 890.
40. J.M. Ziman, *Electrons and Phonons*. Chap. V, p. 175. Oxford University Press, Oxford (1972).

41. T. Theiler, F. Keilmann, and E.E. Haller, *Third Int. Conf. on Shallow Impurities in Semiconductors*, Linkoeping, Sweden (1988).
42. T. Theiler, Ph. D. Thesis, Stuttgart Univ. FRG (1989).
43. J.B. McManus, R. People, R.L. Agarwal, and P.A. Wolff, *J. Appl. Phys.* **52** (1981) 4748.
44. E.M. Conwell, *Solid State Physics.* Supplement 9, F. Seitz, D. Turnbull, and H. Eherenreich, editors. Academic Press N.Y. (1967).
45. H. Navarro, R. Till, T. Theiler and F. Keilmann. To be published (1991).
46. F. Keilmann, *SPIE Far-Infrared Science and Technol.* **666** (1986) 213.
47. R. Till and F. Keilmann, *Fourth Int. Conf. Infrared Physics*, Zurich (1988).
48. G. Ascarelli and S. Rodriguez, *Phys. Rev.* **127** (1962) 167.
49. H.A. Bethe and E. Salpeter, *Quantum Mechanics of One and Two Electron Atoms.* Academic Press, Inc. N.Y. (1957).
50. R.H. Pantell and H.E. Puthoff, *Fundamentals of Quantum Electronics*, p. 71. John Wiley, N.Y. (1969).
51. E.O. Kane, *Phys. Rev.* **119** (1960) 40.
52. J.J. White, *Can. J. Phys.* **45** (1967) 2792.
53. Y. Nisida and K. Horii, *J. Phys. Soc. Japan* **26** (1969) 388.
54. T. Ohyama, *Phys. Status Solidi A* **98** (1980) 373.
55. C. Jagannath, Z.W. Grabowski and A.K. Ramdas, *Phys. Rev. B* **23** (1981) 2082.
56. R. Loudon, *The Quantum Theory of Light.* 1st ed. chap. 3 and 8. Clarendon Press, Oxford (1973).
57. K. Nishikawa and R. Barrie, *Can. J. Phys.* **41** (1963) 1135.
58. R. Barrie and K. Nishikawa, *Can J. Phys.* **41** (1963) 1823.
59. M. Kogan and T.M. Lifshits, *Phys. Stat. Solidi A* **39** (1977) 11.
60. S.N. Artemenko, A.A. Kal'fa, S.M. Kogan and V.I. Sidorov, *Sov. Phys. Semicond.* **8** (1975) 1405.

Resumen. Se presenta una revisión de las propiedades físicas relacionadas con la observación de transiciones entre estados cuánticos electrónicos de impurezas donadoras en material semiconductor de Germanio. Se hace énfasis en la interrelación que la espectroscopia del infrarrojo lejano y el modelo de masas efectivas han tenido en este tema para la observación y predicción con gran precisión de la energía de los estados cuánticos de estas impurezas, lo mismo en cómo el conocimiento de su naturaleza cuántica puede ser usado para predecir y calcular su respuesta a campos incidentes o aplicados. Algunos de los fenómenos discutidos se ilustran con la presentación de resultados teóricos y experimentales no publicados antes. Estos son: la saturación de los coeficientes de absorción de transiciones entre estados de donadores y el cálculo teórico de la respuesta Zeeman de los niveles donadores $2P_{\pm}$, $3P_{\pm}$ y $4P_{\pm}$. También se discuten los agentes físicos que afectan el ancho de línea de las transiciones donadoras. Las mediciones del ancho de línea intrínseco se reinterpretan como determinadas por la envolvente de los estados resultantes del acoplamiento de estados ligados en el nivel donador-fonones, que es producido por la interacción electrón-fonones acústicos a temperaturas diferentes de cero grados Kelvin.